



Elucidation of aniline adsorption–desorption mechanism on various organo–mineral complexes

Yan Ma¹ · Xinyi Wu¹ · Tong Wang¹ · Shengkun Zhou² · Biying Cui¹ · Haoqun Sha¹ · Bowen Lv³ 

Received: 23 September 2022 / Accepted: 28 December 2022 / Published online: 5 January 2023
© The Author(s), under exclusive licence to Springer-Verlag GmbH Germany, part of Springer Nature 2023

Abstract

Complexes formed by organic matter and clay minerals, which are active components of soil systems, play an important role in the migration and transformation of pollutants in nature. In this study, humic-acid–montmorillonite (HA–MT) and humic-acid–kaolin (HA–KL) complexes were prepared, and their structures before and after the adsorption of aniline were analyzed. The aniline adsorption–desorption characteristics of complexes with different clay minerals and varying HA contents were explored using the static adsorption–desorption equilibrium method. Compared with the pristine clay minerals, the flaky and porous structure of the complexes and the aromaticity were enhanced. The adsorption of aniline on the different clay mineral complexes was nonlinear, and the adsorption capacity increased with increasing HA content. Additionally, the adsorption capacity of HA–MT was higher than that of HA–KL. After adsorption, the specific surface area of the complexes decreased, the surfaces became more complicated, and the aromaticity decreased because aniline is primarily adsorption onto the complexes via aromatic rings. Aniline was adsorbed onto the complexes via spontaneous exothermic physical adsorption. The amount of aniline desorbed from the complexes increased with increasing HA content, and a lag in desorption was observed, with a greater lag for HA–KL than for HA–MT.

Keywords Organo–mineral complex · Humic-acid content · Clay minerals · Kinetics · Adsorption models · Desorption hysteresis

Introduction

Aniline, a fundamental industrial amine, and its derivatives are extensively used in various industries such as medicine, agriculture, and the military (Fu et al. 2019). However, the consistent use of aniline and its derivatives has led to their continual and accumulation in the environment through the release of industrial wastewater, accidental leakage, or direct

application to soil, posing considerable risks to the environment and human health. Serious aniline-leakage accidents have occurred in China, which severely threatened the normal lives of surrounding residents (Sun et al. 2015; Mohammed et al. 2020). For example, a previous study reported aniline concentrations of 300–3900 µg/L in alkaline paddy soil in Jiangsu Province, 50–1300 µg/L in river sediment in Guangzhou, and 20–1100 µg/L in sludge from a solid waste yard in Guiyang (Liu et al. 2020). In addition, a chemical plant in Hebei Province discharged untreated wastewater into surrounding ponds, resulting in the aniline concentration in the groundwater reaching 7.33 mg/L, far exceeding the standard limit (Sissou et al. 2019). According to the requirements of the Grade II standard of the Integrated Wastewater Discharge Standard of China (GB 8978–1996), the discharge of aniline in wastewater is ≤ 2 mg/L. The US EPA suggested a 0.262 ppm limit for aniline in water. Therefore, the degradation of aniline to minimize its harmful influence on the surrounding environment is critical.

Various media exist in the soil. Clay minerals and organic matter, the primary active components in soil, significantly

Responsible Editor: Tito Roberto Cadaval Jr

✉ Bowen Lv
bwtt2020@163.com

¹ School of Chemical and Environmental Engineering, China University of Mining & Technology (Beijing), Beijing 100083, People's Republic of China

² Beijing Solid Waste Treatment Co., Ltd, Beijing 100101, People's Republic of China

³ Policy Research Center for Environment and Economy, Ministry of Ecology and Environment, Beijing 100029, People's Republic of China

influence the migration and transformation of organic pollutants in soil (Yang et al. 2021; Cheng et al. 2021). The strong attraction of clay minerals for organic matter results in the formation of stable organo–mineral complexes by filling and combining with minerals. The complexes can change the properties of the mineral surface and the structure of associated organic matter and affect the adsorption capacity of soil for organic pollutants (Zhu et al. 2016; Ren et al. 2021). The organo–mineral complexes also play a key role in stabilizing soil organic carbon (Xu et al. 2022; Georgiou et al. 2022). Various natural minerals with complex structures combine with organic matter in different ways, leading to varying degrees of pollutant adsorption. In particular, kaolin and montmorillonite are extensively used as representative clay minerals owing to their abundance in soil, high specific surface area (SSA), negative surface charge, and cation interaction characteristics (Campos et al. 2013; Xu et al. 2019). Kaolin has a 1:1 layered structure with small interlayer spacing and low organic content (Wang et al. 2018). Montmorillonite has a 2:1 layered structure with an unstable interlayer spacing that changes with the water content, and the surface functional groups are mainly hydroxyl groups (Wang et al. 2020). The structures of organo–mineral complexes containing montmorillonite and kaolin have been characterized by nuclear magnetic resonance (NMR) spectroscopy. Analysis of the ^{13}C and ^1H NMR spectra indicates that the montmorillonite complex first combines with highly saturated amino acids and fatty acids under hydrophobic interactions, whereas kaolin first combines with the fatty acid carbon on chains, while the clay minerals provide protection and fixation for organic matter (Turlapati et al. 2015).

The adsorption of heavy metals and organic pollutants on organic matter or minerals in water and soil has been widely studied (Ruan et al. 2015; Belousov et al. 2019; Qian et al. 2022). Additionally, the adsorption characteristics and mechanisms of organic pollutants in soil by organo–mineral complexes are being explored. Pollutant adsorption by these complexes in the soil is affected by the type of clay mineral, initial concentration of the adsorbate, and proportion of organic matter in the clay minerals (Huang et al. 2015). The adsorption mechanism depends on the properties of the pollutant and organo–mineral complex and their interactions. The specific adsorption mechanism determines the extent of migration and transformation of the pollutants in the soil. Molecular dynamics analysis has revealed that humic acid (HA) can increase the adsorption of pollutants by organo–mineral complexes by forming hydrogen-bond networks with glyphosate and kaolinite (Guo et al. 2021). Factors such as the type of mineral and its properties, interlayer charge, and carboxylic acid groups significantly influence the interaction mechanism between organic carbon and minerals in soil under natural conditions. The structure and content

of organic matter before and after the preparation of organo–mineral complexes was examined by synthesizing an HA–nano-ferric-oxide complex (Peng et al. 2015). The physical and chemical properties of HA were dependent on the ofloxacin and norfloxacin adsorption capacities of the complex. However, research on the physicochemical properties of organic matter and clay minerals and their composites with various proportions is lacking. Moreover, the influence of organo–mineral complexes on the adsorption–desorption characteristics of organic pollutants has not yet been comprehensively elucidated.

To address these gaps in the knowledge, HA and montmorillonite/kaolin (MT/KL) were used to simulate soil organic matter and clay minerals, respectively, in this study. Additionally, HA–MT and HA–KL complexes with different clay materials and organo–mineral ratios were prepared. Static adsorption equilibrium tests were performed, and the morphology, porosity, and chemical properties of the materials were characterized. The purpose of this study was to clarify the dominant mechanism by which the soil organic matter–clay mineral complex affects the adsorption and desorption of organic pollutants. The study can contribute to the evaluation and prediction of the potential risks of aniline soil pollution and to the development of improved soil-remediation strategies.

Materials and methods

Sample preparation

Aniline ($\text{C}_6\text{H}_7\text{N}$) and MT ($\text{Al}_2\text{O}_9\text{Si}_3$) were purchased from McLean Pharmaceutical Company. KL ($\text{Al}_2\text{Si}_2\text{O}_5(\text{OH})_4/\text{H}_2\text{Al}_2\text{Si}_2\text{O}_6\cdot\text{H}_2\text{O}$) and nitric acid (HNO_3) were purchased from Sinopharm Chemical Reagents, while HA ($\text{C}_9\text{H}_9\text{NO}_6$) and NaOH were purchased from Alfa Aesar (China) and Beijing Tongguang Fine Chemical Company, respectively.

HA (0 g, 1 g, 2 g, 3 g, 4 g, and 5 g) was dissolved in ultrapure water, and MT (50 g) was added to each portion. The pH of the resulting solutions was adjusted to 9 using NaOH and HNO_3 solutions (1 mol/L). The mixed suspending liquid was manually stirred for 1 min, placed in a constant-temperature oscillation incubator, agitated for 24 h at 200 rpm at room temperature (20–25 °C), and subsequently centrifuged at 3500 rpm. The supernatant was removed and frozen in a refrigerator for 48 h, freeze-dried for an additional 48 h, and filtered through a 250-mesh sieve. The resulting samples were then sealed and stored inside a container. These samples are henceforth denoted according to the weight ratio of HA to MT (0%, 2%, 4%, 6%, 8%, and 10% HA–MT). The HA–KL complexes were similarly prepared.

Characterization

The structures of the pristine and aniline-adsorbed organo–mineral complexes and their components were characterized. The surface morphology of the soil particles and their elemental composition in a vacuum were investigated by scanning electron microscopy (SEM) and energy-dispersive X-ray spectroscopy (EDS). The influence of the organo-matter–clay-mineral interactions on their respective structural characteristics was investigated by determining the SSA via Brunauer–Emmett–Teller (BET) analysis. Infrared spectroscopy with full-band scanning was performed (Nicolet6700; Thermo Fisher China). XPS analysis was performed to determine the surface elemental compositions of the pristine soil samples. An electron probe was used to analyze the elemental distribution on the mineral surface and obtain images of the organo–mineral complexes. The influence of the unique functional groups of HA in the complexes on their adsorption–desorption behavior was quantitatively analyzed by NMR spectroscopy (Bruker AU300; Switzerland).

Batch adsorption–desorption experiments

The batch static adsorption–desorption equilibrium method was used in this study. First, aniline stock solutions with concentrations of 100 µg/L, 200 µg/L, 400 µg/L, 800 µg/L, 1200 µg/L, 1600 µg/L, and 2000 µg/L were prepared. An HA–MT simulated soil sample (50 mg) and aniline stock solution (20 mL) were added to a centrifuge tube (50 mL). The sample was quickly covered, sealed, stored away from light, and subsequently placed in a constant-temperature air-bath oscillator. Gas chromatography (GC) was used to determine the aniline concentration. The sample was placed in the headspace column. The Rtx-5 column was used (30 m × 0.25 mm × 0.25 µm), along with a flame ionization detector (FID). The GC operating conditions included an injection volume of 1 µL, split ratio of 200:1, constant column temperature of 80 °C, flow rate in the chromatographic column of 3 mL/min, sample inlet temperature of 150 °C, detector temperature of 250 °C, exhaust flow rate of 30 mL/min, hydrogen flow rate of 40 mL/min, and air flow rate of 400 mL/min. Because of a large number of samples prepared, the 4% HA–MT and 4% HA–KL complexes were used to determine the aniline adsorption equilibrium time using aniline solutions with initial concentrations of 800 µg/L and 1600 µg/L based on the environmental concentration and previous studies (Liu et al. 2020). The adsorption equilibrium time of aniline was determined by the oscillating balance method. A prepared soil sample (50 mg) was accurately weighed into a 50-mL centrifuge tube, and 20 mL of aniline solution was injected quickly. To avoid light, the tube was wrapped in aluminum foil. A centrifuge tube without a sample was used as a control sample, and it was centrifuged at 25 °C and 160 rpm. The tubes were

removed from the centrifuge after 0 h, 1 h, 2 h, 4 h, 8 h, 12 h, 24 h, and 48 h, respectively. Two parallel samples were taken, which were centrifuged at 6000 rpm for 10 min. We took 1 mL of supernatant from the headspace bottle which was tested using GC to determine the concentration of residual aniline in the solution and determine the adsorption equilibrium time. Three parallel experiments were conducted for each group, and the standard sample without adsorbent was used as the control. Supplementary Fig. S1 shows the concentration vs. time curves from which an adsorption equilibrium time of aniline of 24 h was obtained. To ensure adsorption equilibrium in the solution, an equilibration time of 48 h was used in the experiments. After this time, the tube was centrifuged at 6000 rpm for 10 min. The supernatant (1 mL) was passed through a 0.45-µm filter membrane using a syringe and quickly injected into a headspace bottle (2 mL), sealed with a pressure cap, and analyzed. The aniline concentration after adsorption equilibrium (C_e) was recorded, and three parallel experiments were performed in each group using a complex-free standard sample as the control. Various kinetic models—pseudo-first-order, pseudo-second-order, Elovich, and intraparticle diffusion models—were used to fit the adsorption data (Chianese et al. 2020).

The aniline desorption experiments were performed based on the results of the adsorption experiments, with an aniline desorption equilibrium time of 48 h. After the adsorption experiments were performed, each sample was centrifuged at 6000 rpm for 10 min to separate the solid from the liquid. After treatment under dark conditions, each sample was placed in a centrifuge tube in an oscillator at 160 rpm and oscillated at a constant temperature for 48 h until desorption equilibrium was achieved. The top-empty bottle was centrifuged for 10 min at 6000 rpm. Subsequently, the supernatant (1 mL) was added to a top-empty bottle, which was placed in the GC instrument to determine the final desorption equilibrium concentration of aniline (C'_e). Three sets of parallel experiments were conducted in each group using an absorbent-free standard sample as the control.

Data analysis

The adsorption and desorption data were fitted using the linear, Langmuir, and Freundlich models. The aniline adsorption and desorption capacities of the complexes were calculated using Eqs. (1) and (2), respectively.

$$Q_e = \frac{(C_0 - C_e)V}{m} \quad (1)$$

$$Q_e^{des} = \frac{(C'_e - C_e)V}{m} \quad (2)$$

Here, Q_e ($\mu\text{g/g}$) is the amount of aniline adsorbed by the complexes, C_0 ($\mu\text{g/L}$) is the initial concentration, C_e ($\mu\text{g/L}$) is the concentration at adsorption equilibrium, Q_e^{des} ($\mu\text{g/g}$) is the fraction of solid-phase desorption of aniline by the complexes, C_e' ($\mu\text{g/L}$) is the aniline concentration at desorption equilibrium, m (g) is the mass of the complex, and V (L) is the solution volume.

Adsorption isotherm data collected at different temperatures were fit to determine the adsorption coefficient (K). Thermodynamic parameters such as changes in the Gibbs free energy [ΔG ($\text{kJ}\cdot\text{mol}^{-1}$)], enthalpy [ΔH ($\text{kJ}\cdot\text{mol}^{-1}$)], and entropy [ΔS ($\text{kJ}\cdot\text{mol}^{-1}\cdot\text{K}^{-1}$)] were calculated as follows:

$$\Delta G = -RT \ln K \quad (3)$$

$$\ln K = -\frac{\Delta H}{RT} + \frac{\Delta S}{R} \quad (4)$$

$$\Delta G = \Delta H - T\Delta S \quad (5)$$

Results and discussion

Characterization of complexes

SEM analysis identified the presence of 1- μm block-like HA and a high degree of aggregation of small particles. The structure of pristine HA was dense. The surface had a microporous structure with small pores and a smooth surface owing to pore filling. The major elements were C and O,

with minor amounts of Al and Si. Based on this, the macromolecular structure of HA was thought to mainly contain aromatic and alicyclic rings. KL had a granular structure, which may enable satisfactory ion exchange and adsorption. The main components of KL were O, Al, and Si, consistent with previous results (Wen et al. 2019). SEM performed at 1000 \times magnification revealed that MT had the lamellar structure of clastic scales, and the spacing between scales is relatively small; moreover, MT contained O, Si, and Al as the primary components.

A comparison of the surface morphologies of the soil samples before and after forming complexes reveals that the surfaces of the complexes were uneven and the pore structures were more obvious than those in the initial clay. No obvious changes were found in the major constituent elements of HA–MT at the investigated site; however, the C content of HA–KL increased (Fig. 1). The complexes formed by the two minerals were in the form of flaky polymers, similar to the surface morphologies of MT and KL. The formation of these complexes was presumably influenced by the clay minerals—MT and KL—and the links between small granular HA and the mineral surfaces. EDS maps (Supplementary Fig. S2) show that the C signal from the two complexes was very high at the edge of the particles but extremely low in their interior, indicating that HA was adsorbed primarily on the clay mineral surfaces, with the tiny HA particles possibly entering the pores of the clay.

Macromolecular organic matter (such as HA) and other components are known to be readily adsorbed on the surface of clay minerals, which is dependent on the surface structure of the minerals, such as their SSA and pore volume

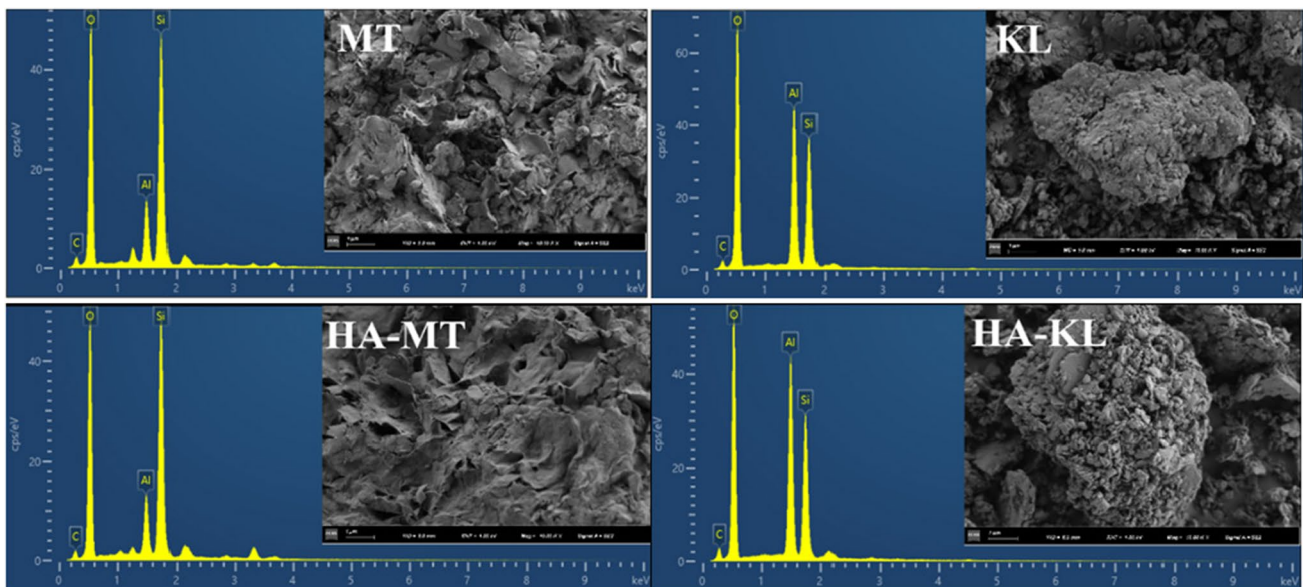


Fig. 1 SEM-EDS images of MT, KL, and HA–MT and HA–KL complexes (scale bar: 1 μm)

(El-Sayed et al. 2019b; Qu et al. 2019; Chen et al. 2017). The properties of different organo-mineral complexes prepared in previous studies also have certain differences, which are compared in Supplementary Table S1. Owing to the large number of samples prepared in this study, specimens with 4% HA and similar contents of the two mineral types were selected for characterization. Analysis of the pore characteristics of the simulated soil revealed that MT and HA had the largest (54.421 m²/g) and smallest (4.938 m²/g) SSA values, respectively (Table 1). The SSA values of the two complexes changed upon the addition of MT or KL to HA, with the SSA values of the HA–MT and HA–KL decreasing and increasing compared with the original MT and KL, respectively. The adhesion of HA to the surface of the framework of minerals during its combination with the minerals possibly led to the reduction in the SSA of HA–MT.

The IR spectra of HA, MT, and KL suggested several similar molecular structures (Fig. 2a). The six pre- and post-complexing samples were similar in structure that contained abundant functional groups, such as hydroxyl, aliphatic hydrocarbon, carboxyl, carbonyl, and aromatic structures. The addition of HA to the clays did not significantly alter the overall structure of the clay minerals (Sabah and Ouki 2017). Distinct peaks corresponding to –OH stretching vibration, mineral absorption, C=C stretching vibration of the aromatic ring skeleton, and Si–O stretching vibration were observed at 3500–3430 cm⁻¹, 3622 cm⁻¹, 1640–1570 cm⁻¹, and 1030 cm⁻¹, respectively, although with different intensities. The complexes exhibited intense absorption peaks related to carbonyl stretching between 1100 and 1030 cm⁻¹, indicating considerable changes in the C–O absorption peaks of the clay minerals after complexation.

XPS analysis showed that the surfaces of KL, MT, and their complexes with HA contained elements such as C, O, Al, and Si (Fig. 2b). Additionally, a small peak corresponding to the binding energy of Mg1s was observed in the spectra of MT and its complexes at 1303 eV, indicating that their surfaces also contained small amounts of Mg. The elemental compositions of 4% and 10% HA–MT were very similar; however, the fractions of C and O in 10% HA–MT were slightly higher than those in 4% HA–MT due to the

additional C and O provided by the higher HA content. This result is also consistent with the increase in the number of C–O functional groups concluded from IR analysis. Electron probe analysis (Supplementary Fig. S3) revealed that both complexes had a layered structure; moreover, the complexes were scanned based on their Al, Si, C, and O contents. The surface of 4% HA–KL was rich in Al, Si, and O, whereas that of HA–MT had lower Al and higher Si and O contents, indicating the presence of numerous silicate minerals on the surfaces of the two complexes and the presence of several aluminates on the surface of HA–KL; this corroborates the results obtained from SEM and XPS analyses of the complexes.

Adsorption of aniline by organo–mineral complexes

Adsorption isotherms and kinetics

The aniline adsorption kinetic curves of complexes with different clay mineral types toward two different initial concentrations of aniline were collected (Fig. 3a). The reaction time, initial concentration of aniline, and clay mineral type significantly influenced the adsorption kinetics. The adsorption of aniline on the organo–mineral complexes involved a rapid increase, a slow increase, and eventual stabilization. These trends may be related to the adsorption sites on the surface of the complex (Guo et al. 2016). Because of the limited number of surface adsorption sites, the adsorption sites are continuously occupied by aniline over time, resulting in fewer sites for subsequent adsorption of aniline on the surfaces of the soil organic components. This is observed as a decrease in the adsorption rate, up to the point where the aniline adsorption sites are exhausted and the concentration plateaus. The pseudo-first-order, pseudo-second-order, Elovich, and intraparticle diffusion kinetic models were used to fit the aniline adsorption data of the aforementioned complexes, and the fitting parameters were obtained (Supplementary Table S2). The adsorption rate constant, K_1 , values suggest that the adsorption capacity of HA–MT was higher than that of HA–KL. The data were the best fit by the

Table 1 Porosity-related parameters of simulated soil samples

Sample	Specific surface area (SSA _{BET} ; m ² /g)	Pore capacity (cm ³ /g)	Pore size (nm)
HA	4.938	0.003	2.714
MT	54.421	0.122	8.931
KL	10.286	0.029	11.36
4% HA–MT	50.137	0.143	8.201
4% HA–KL	14.366	0.043	11.841
4% HA–MT (after adsorption)	14.937	0.0395	10.580
4% HA–KL (after adsorption)	10.455	0.0490	12.630

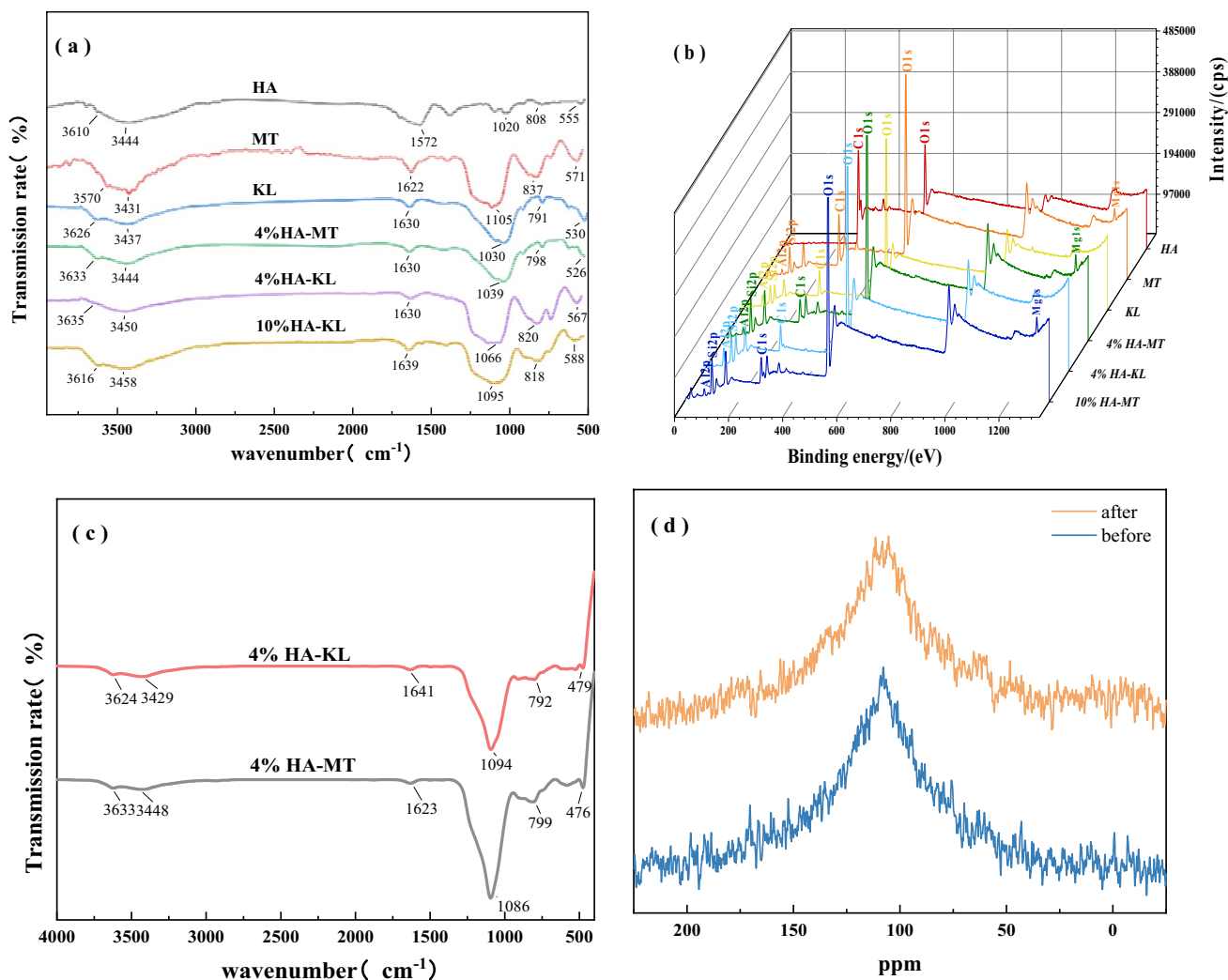


Fig. 2 Characterization of initial materials and complexes. **(a)** IR spectra. **(b)** Full-spectrum XPS scans. **(c)** IR spectra of two complexes after aniline adsorption. **(d)** ^{13}C -NMR spectra of the 4% HA–MT complex before and after adsorption

pseudo-second-order kinetic model (Fig. 3b), proving that the adsorption of aniline on the organo–mineral complexes was driven by the dominant active sites on the surface rather than the concentration of aniline in the solution (Sander and Pignatello 2005; Lu et al. 2018). Additionally, the adsorption of aniline on the complexes possibly involved the internal diffusion of particles, surface adsorption, and liquid-film diffusion (El-Sayed et al. 2019a). The clearly different Q_e values of the different complexes were presumably due to their SSA values and pore volumes, which can provide a larger contact area and more adsorption sites for aniline adsorption (Zhang et al. 2010). The fitting effect of the Elovich model is second only to that of the pseudo-second-order kinetic equation, which indicates that the adsorption of aniline on the surface of the complex also has a heterogeneous diffusion process. Additionally, the constant (C) corresponding to the intraparticle

diffusion rate of 4% HA–KL was relatively large, suggesting a significant influence of liquid-film diffusion on the adsorption rate.

Effects of temperature on aniline adsorption by the complexes

The effects of different temperatures (288 K, 298 K, and 308 K) on aniline adsorption by the complexes were studied. The Q_e of aniline decreased with increasing temperature in the reaction system (Supplementary Fig. S4), indicating that higher temperatures did not facilitate aniline adsorption on the organo–mineral complexes. When the initial adsorption concentration was 400 $\mu\text{g/L}$, the aniline adsorption capacity of 4% HA–MT decreased from 39.92 to 33.12 $\mu\text{g/L}$ as the temperature increased from 288 to 308 K, respectively, due to the influence of temperature on aniline adsorption.

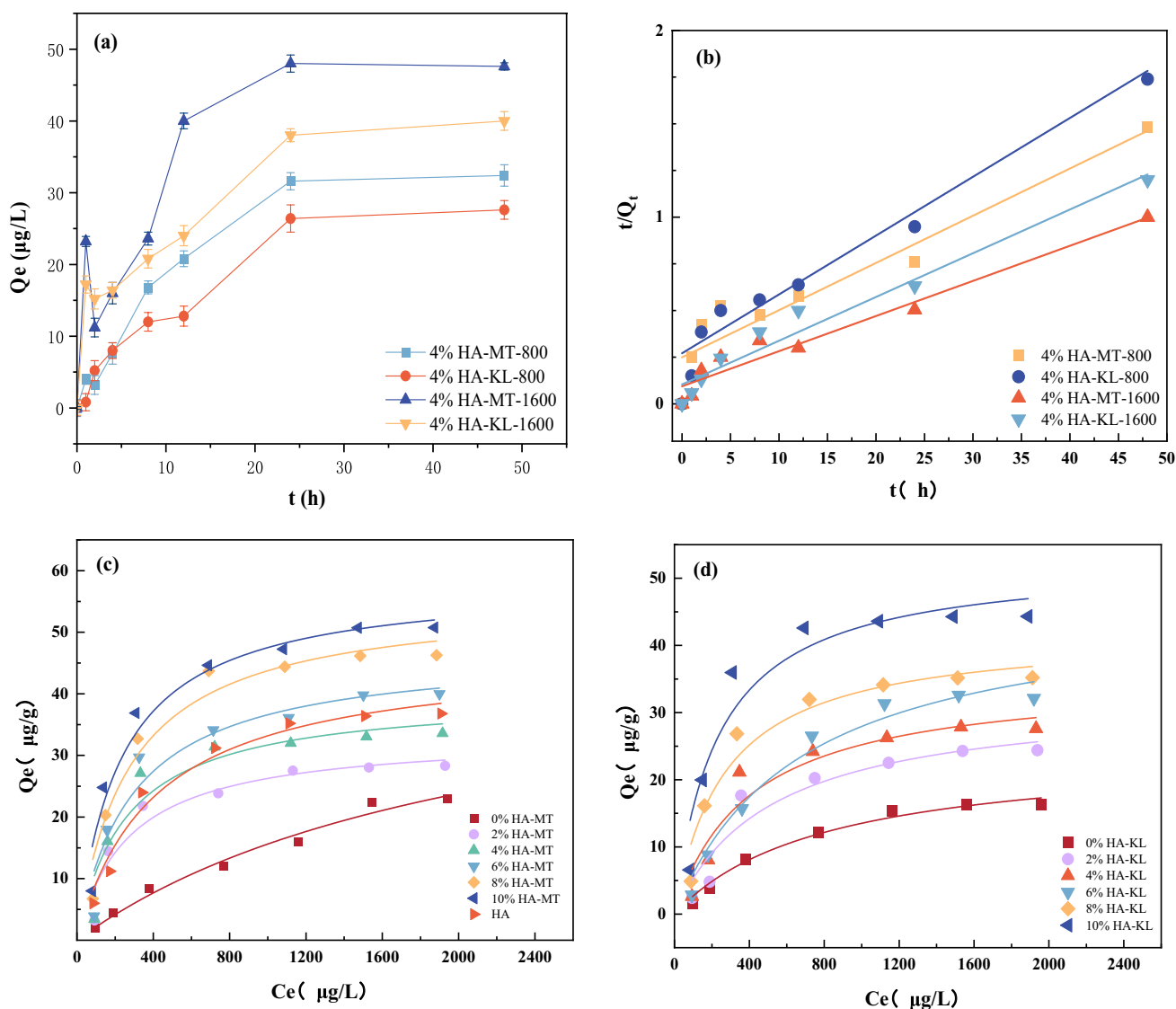


Fig. 3 Fits of kinetic models to the adsorption data. (a) Kinetics of aniline adsorption on soil samples (the aniline concentration is 800 µg/L and 1600 µg/L). (b) Pseudo-second-order dynamic fitting curves. Langmuir model fits of aniline adsorption on (c) HA and HA–MT and (d) HA–KL

The solubility of aniline increases with increasing temperature, weakening the aniline–complex interactions and consequently impeding its adsorption (Zhou et al. 2015). The Langmuir equation was also used to fit the aniline adsorption data of the complexes. The fitting parameters indicate the monolayer adsorption of aniline on the complexes (Supplementary Table S3).

The thermodynamic parameters of the adsorption are listed in Supplementary Table S4. According to the change in adsorption enthalpy (Von Oepen et al. 1991) caused by different forces ($|\Delta H| < 40 \text{ kJ}\cdot\text{mol}^{-1}$), the adsorption of aniline on the complexes primarily depends on van der Waals forces. $|\Delta H|$ values in the ranges of 2.1–20.9 $\text{kJ}\cdot\text{mol}^{-1}$ and 80–200 $\text{kJ}\cdot\text{mol}^{-1}$ represent physical and chemical adsorption, respectively (Yousef et al. 2011). The value of $|\Delta H|$

in the present study ($6.46 \text{ kJ}\cdot\text{mol}^{-1}$) indicates the physical adsorption of aniline on the complexes. Additionally, the negative values of the changes in the Gibbs free energy, enthalpy, and entropy of aniline at different temperatures indicate that the adsorption of aniline by the complexes was spontaneous and exothermic (Tang et al. 2019).

Effects of mineral type and HA content on aniline adsorption

Adsorption isotherms were used to evaluate the adsorption capacities of the simulated soil samples and elucidate the organo–mineral complex and aniline interaction mechanism. Different organic-matter/clay-mineral ratios can also affect the HA–mineral binding mechanism. During

the complexation of MT or KL with HA, the interaction mechanisms of MT and KL are different owing to their distinct structures and HA contents. Three models were used to fit the aniline adsorption data of 10 different complexes (0–10% HA–MT and 0–10% HA–KL) and HA (Supplementary Table S5). The fits to the experimental data clearly indicate nonlinear adsorption. The adsorption capacity of the prepared complexes was higher than that of HA, presumably because of the increase in its SSA and aromatic carbon content after complexation. The slope of the adsorption isotherm gradually decreased, and the adsorption capacity of all soil samples steadily increased with increasing Q_e of aniline. This phenomenon is possibly related to the heterogeneity of the surface energy of the complex. The aniline in the adsorption reaction medium first occupies the high-energy sites on the organo–mineral complex surface and subsequently combines with the lower-energy sites upon saturation of the high-energy sites. The Langmuir isothermal adsorption model, rather than the Freundlich model, describes the entire isothermal adsorption of aniline in solution on the organo–mineral complex surface; additionally, the maximum adsorption capacity estimated by this model predicted the theoretical saturated aniline adsorption capacity of the soil (Fig. 3c, d). However, previous studies have also shown that increasing the HA content in complexes reduces the adsorption of pollutants, possibly due to electrostatic repulsion between the adsorbed HA and pollutants (Arroyave et al. 2016).

After HA occupies the adsorption sites on the surfaces of KL and MT, sparse molecular layers of HA are formed on the mineral surfaces. However, HA is not uniformly attached to the mineral surfaces, but is irregularly distributed on their adsorption sites, thus increasing the number of adsorption sites for organic pollutant adsorption (Li et al. 2022). Therefore, the adsorption capacity gradually increased with increasing HA content. The aromatic components of HA are known to combine with KL through the intercalation effect, and free carboxyl groups interact on the surface of KL to form dense carbonaceous patches with a mineral core and dense outer layer (Wang et al. 2018). Generally, pollutant adsorption on organo–mineral complexes is related to their SSA; a larger SSA provides more adsorption sites, enhancing the adsorption capacity for organic pollutants. The experimental adsorption data suggest that the adsorption capacity of the HA–MT was higher than that of the HA–KL, which is consistent with the larger SSA values of the HA–MT than that of HA–KL.

Mechanism of aniline adsorption by organo–mineral complexes

The SSA values of HA–MT and HA–KL were considerably reduced after aniline adsorption (Table 1); the number

of exchangeable sites decreased, and the adsorption capacity weakened. This was possibly due to the plugging of the surface pores of the complexes with aniline molecules, which decreased the SSA, total pore volume, and average pore size. The action of polar water molecules on the surface of the clay minerals could also be responsible. When organic pollutant molecules are in contact with inorganic minerals, the pollutants first replace water molecules on the surface of the minerals (Sun et al. 2020). Fitting the adsorption isotherms of aniline with different models showed that the adsorption of aniline on the organo–mineral complexes is driven by the main active sites on the surface. In addition, heterogeneous diffusion occurs during adsorption, and liquid-film diffusion has a significant effect on the adsorption rate.

SEM analysis conducted at 10,000× magnification (Fig. 4) indicated that HA–KL and HA–MT had clear flake structures that were remarkably different from those of their components prior to the preparation. The surfaces of the complexes after adsorption were more complex pore structures, the pore size was clearly reduced, and the HA particles were covered by a film or crumb-like substance that concealed the bulk particle. After adsorption, aniline was attached to the complex, and the pores were gradually filled. The IR spectra (Fig. 2c) indicate that the contents of aromatic rings and substituted aromatic rings in the complexes before adsorption were higher, followed by those of N–H bonds or hydrogen bonds between the N–H bonds and other atoms in the complexes; the characteristic peaks of the latter disappeared or diminished after aniline adsorption, indicating that interactions between these functional groups and aniline occurred during adsorption. Single absorption peaks were observed at 3429 cm^{-1} and 3448 cm^{-1} , which correspond primarily to the stretching vibration of R–OH or –NH. Additionally, a wide and intense vibration band appeared after adsorption. Peaks representing the C=C vibrations of the olefin group, C=O of the conjugated ketone group on the aromatic carbon, or the symmetric stretching of carboxyl –COOH were observed at 1623 cm^{-1} and 1641 cm^{-1} . Therefore, aniline was adsorbed onto the complexes primarily through the aromatic rings and secondarily through N–H bonds. The NMR results (Fig. 2d) reveal that the 4% HA–MT complex did not exhibit obvious changes after adsorption, and the complex consisted of aromatic and fatty carbons. The complex had hydrocarbon chains and aromatic carbon as the skeleton and several oxygen- and nitrogen-containing functional groups. The relative content of each component in the complex was determined by integrating each spectral interval. The ^{13}C signal of HA–MT spanned the aforementioned organic regions. After adsorption, the aromaticity of the complex weakened, while the alkyl carbon content increased.

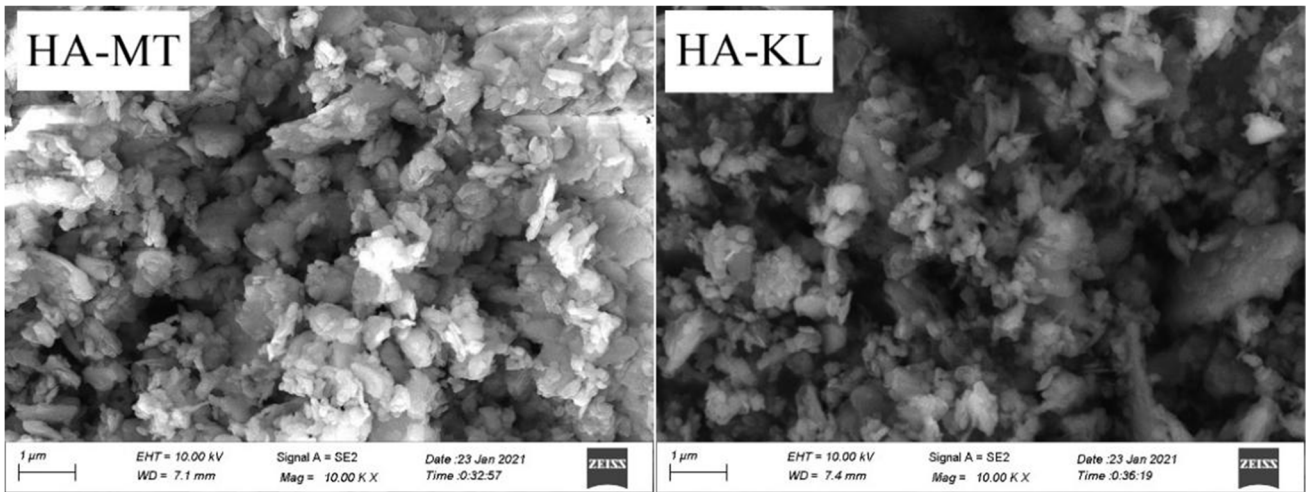


Fig. 4 SEM images of the complexes after absorption (scale bar: 1 μm)

Desorption of aniline from organo–mineral complexes

Effects of humic acid content on aniline desorption from complexes

The Langmuir model was used to fit the aniline desorption data of complexes with different HA contents (Fig. 5). The amount of aniline desorbed from the complexes was low, and the adsorption–desorption characteristics of the different complexes varied. Moreover, the lack of overlap between the adsorption and desorption isotherms indicated that desorption lagged behind adsorption. The amount of aniline desorbed by the complexes increased with increasing

equilibrium concentration of aniline. The addition of a certain amount of HA promoted aniline desorption from the complex. This is possibly due to the increasing aniline adsorption capacity of the complexes with increasing HA content, which increased the desorption capacity (Yeasmin et al. 2014).

Investigation of desorption hysteresis

Desorption lag, which is expressed by the hysteresis index (HI), occurs at $HI < 0.7$ and does not occur at $HI = 0.7–1.0$; moreover, the adsorbent can readily desorb at $HI > 1$ (Doretto and Rath. 2013). The aniline adsorption–desorption data of the complexes were fit using the Freundlich

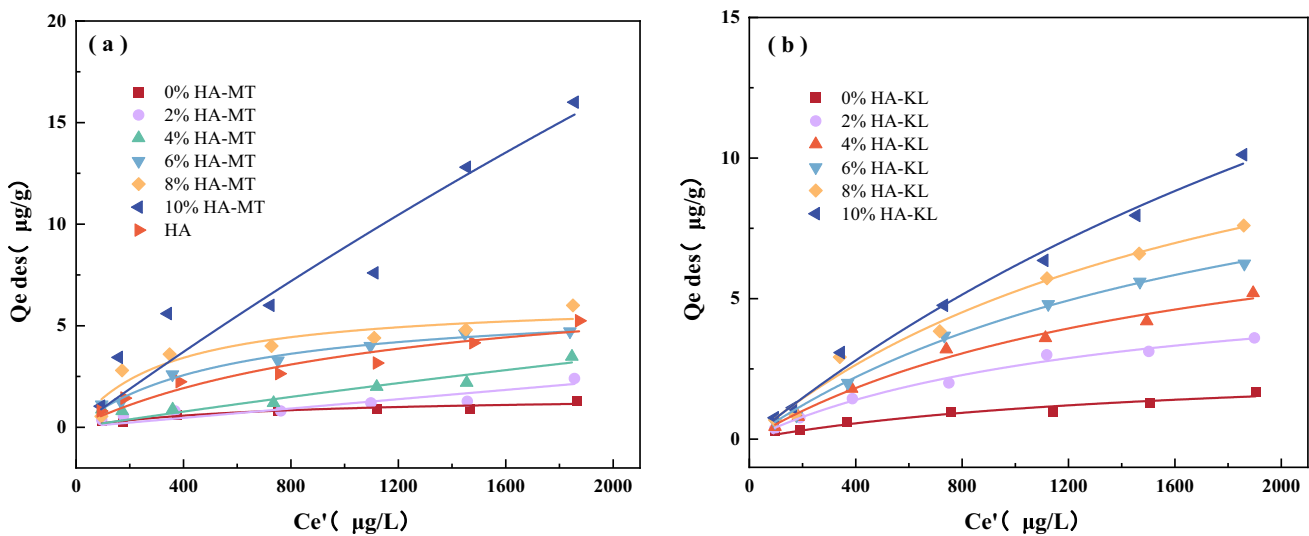


Fig. 5 Langmuir model fits of aniline desorption from (a) HA and HA–MT and (b) HA–KL

isothermal model to further examine the degree of influence of the aniline adsorption–desorption lag of the MT complexes. Supplementary Table S6 shows the Freundlich model fits and the desorption lag of aniline adsorption–desorption of the complexes. The HI values of HA–MT complexes for aniline desorption ranged from -0.500 to 0.535 , which are all less than 0.7 , indicating desorption hysteresis, the degree of which depended on the HA content of the HA–MT complex. The HI of the HA–MT complexes for aniline desorption increased with increasing HA content, indicating that the nonlinear characteristics of the adsorption reaction and the hysteresis of the desorption reaction were related to the HA content and that the adsorption capacity increased with increasing HA content. In addition, the smallest HI corresponded to 0% HA–MT, indicating that aniline desorption from pure MT was the most difficult, which confirms with the change of desorption amount in the above desorption results. Additionally, a lag was observed in the desorption of aniline from HA–KL. The corresponding HI values were between -0.384 and 0.425 (i.e., < 1), indicating that aniline desorption from HA–KL is difficult. Similar to the case for the MT complexes, higher HA contents resulted in higher adsorption/desorption capacities of HA–KL. Although both complexes showed desorption lag, the HI values of HA–MT were generally greater than that of HA–KL at similar HA contents.

Conclusion

This study reveals the aniline adsorption mechanism of organo–mineral complexes, which provides an important theoretical basis for the migration and transformation process of aniline in soil. The aniline adsorption–desorption characteristics and mechanisms of complexes with different mineral types and HA contents were explored. The Langmuir model showed the best fit for the adsorption data. Thermodynamic analysis of the aniline adsorption indicated spontaneous exothermic physical adsorption. Aniline adsorption was dependent on the type of mineral complex, and the adsorption capacity of the HA–MT complexes was higher than that of HA–KL. Additionally, aniline was adsorbed primarily through interactions between the aromatic rings and complexes. The aniline adsorption–desorption capacity of the two complexes increased with increasing HA content. Understanding the adsorption characteristics of aniline in organo–mineral complexes and the adsorption mechanism is very important for predicting and evaluating the potential hazards of aniline pollution of soil and for carrying out soil remediation. The soil environment is complex, and there are many influencing factors, such as the presence of metal ions and microorganisms. Future research could focus on studying the interaction between pollutants and

organo–mineral complexes by taking real samples to better understand the fate of pollutants in the soil.

Supplementary Information The online version contains supplementary material available at <https://doi.org/10.1007/s11356-022-25096-w>.

Acknowledgements We appreciate the efforts of all the researchers whose articles were included in this study. The authors would like to thank the editor and anonymous reviewers for their constructive comments and suggestions for improving the manuscript.

Author contribution All authors contributed to the study's conception and design. Methodology, project administration, and writing – review and editing – were performed by Yan Ma. Investigation, methodology, and writing – original draft – were performed by Xinyi Wu. Investigation, material preparation, data collection, and analysis were performed by Tong Wang. Investigation and writing – review and editing – were performed by Shengkun Zhou. Methodology and visualization were performed by Biying Cui. Investigation and writing – review and editing – were performed by Haoqun Sha. Conceptualization, formal analysis, and supervision were performed by Bowen Lv.

Funding This work was supported by the National Natural Science Foundation of China [grant number 41701353]; the Yue Qi Young Scholar Project, China University of Mining & Technology, Beijing [grant number 2019QN09]; and the National Innovative Experiment Program for College Students of China [grant number 202103050].

Data availability All data and materials generated or analyzed during this study are available from the corresponding author upon reasonable request.

Declarations

Ethics approval and consent to participate Not applicable.

Consent for publication Not applicable.

Competing interests The authors declare no competing interests.

References

- Arroyave JM, Waiman CC, Zanini GP, Avena MJ (2016) Effect of humic acid on the adsorption/desorption behavior of glyphosate on goethite. *Isotherms Kinetics Chemosphere* 145:34–41. <https://doi.org/10.1016/j.chemosphere.2015.11.082>
- Belousov P, Semenikova A, Egorova T, Romanchuk A, Zakusin S, Dorzhieva O, Tyupina E, Izosimova Y, Tolpeshta I, Chernov M, Krupskaya V (2019) Cesium sorption and desorption on glauconite, bentonite, zeolite and diatomite. *Minerals* 9(10):625. <https://doi.org/10.3390/min9100625>
- Campos B, Aguilar-Carrillo J, Algarra M, Gonçalves MA, Rodríguez-Castellón ED, Silva JCG, Bobos I (2013) Adsorption of uranyl ions on kaolinite, montmorillonite, humic acid and composite clay material. *Appl Clay Sci* 85:53–63. <https://doi.org/10.1016/j.clay.2013.08.046>
- Chen H, Koopal LK, Xiong J, Avena M, Tan W (2017) Mechanisms of soil humic acid adsorption onto montmorillonite and kaolinite. *J Colloid Interface Sci* 504:457–467. <https://doi.org/10.1016/j.jcis.2017.05.078>
- Cheng J, Ye Q, Lu Z, Zhang J, Zeng L, Parikh SJ, Ma W, Tang C, Xu J, He Y (2021) Quantification of the sorption of organic pollutants to minerals via an improved mathematical model accounting for

- associations between minerals and soil organic matter. *Environ Pollut* 280:116991. <https://doi.org/10.1016/j.envpol.2021.116991>
- Chianese S, Fenti A, Iovino P, Musmarra D, Salvestrini S (2020) Sorption of organic pollutants by humic acids: a review. *Molecules* 25(4):918. <https://doi.org/10.3390/molecules25040918>
- Doretto KM, Rath S (2013) Sorption of sulfadiazine on Brazilian soils. *Chemosphere* 90(6):2027–2034. <https://doi.org/10.1016/j.chemosphere.2012.10.084>
- El-Sayed MEA, Khalaf MMR, Gibson D, Rice JA (2019a) Assessment of clay mineral selectivity for adsorption of aliphatic/aromatic humic acid fraction. *Chem Geol* 511:21–27. <https://doi.org/10.1016/j.chemgeo.2019.02.034>
- El-Sayed MEA, Khalaf MMR, Rice JA (2019b) Isotherm and kinetic studies on the adsorption of humic acid molecular size fractions onto clay minerals. *Acta Geochimica* 38(6):863–871. <https://doi.org/10.1007/s11631-019-00330-4>
- Fu Z, He N, Zhou P, Xie H, Fu Z, Liu C, Chen J (2019) Grand canonical Monte Carlo simulation on adsorption of aniline on the ice surface. *J Mol Liq* 290:111221. <https://doi.org/10.1016/j.molliq.2019.111221>
- Georgiou, K, Jackson, RB, Vinduškova, O, Abramoff, RZ, Ahlström A, Feng W, Harden JW, Pellegrini AFA, Polley HW, Soong JL, Riley WJ, Torn MS (2022) Global stocks and capacity of mineral-associated soil organic carbon. *Nat Commun* 13(1). <https://doi.org/10.1038/s41467-022-31540-9>
- Guo F, Zhou M, Xu J, Fein JB, Yu Q, Wang Y, Huang Q, Rong X (2021) Glyphosate adsorption onto kaolinite and kaolinite-humic acid composites: experimental and molecular dynamics studies. *Chemosphere* 263:127979. <https://doi.org/10.1016/j.chemosphere.2020.127979>
- Guo X, Tu B, Ge J, Yang C, Song X, Dang Z (2016) Sorption of tylosin and sulfamethazine on solid humic acid. *J Environ Sci* 43:208–215. <https://doi.org/10.1016/j.jes.2015.10.020>
- Huang Y, Liu Z, He Y, Li Y (2015) Impact of soil primary size fractions on sorption and desorption of atrazine on organo-mineral fractions. *Environ Sci Pollut Res* 22(6):4396–4405. <https://doi.org/10.1007/s11356-014-3684-z>
- Liu H, Lin H, Song B, Sun X, Xu R, Kong T, Xu F, Li B, Sun W (2020) Stable-isotope probing coupled with high-throughput sequencing reveals bacterial taxa capable of degrading aniline at three contaminated sites with contrasting pH. *Sci Total Environ* 771:144807. <https://doi.org/10.1016/j.scitotenv.2020.144807>
- Li Y, Koopal LK, Tan W, Chai Y, Chen Y, Wu C, Tang X (2022) Effect of humic acid on lysozyme interaction with montmorillonite and kaolinite. *Sci Total Environ* 834:155370. <https://doi.org/10.1016/j.scitotenv.2022.155370>
- Lu H, Wang J, Li F, Huang X, Tian B, Hao H (2018) Highly efficient and reusable montmorillonite/Fe₃O₄/humic acid nanocomposites for simultaneous removal of Cr (VI) and aniline. *Nanomaterials* 8(7):537. <https://doi.org/10.3390/nano8070537>
- Mohammed M, Mekala LP, Chintalapati S, Chintalapati VR (2020) New insights into aniline toxicity: aniline exposure triggers envelope stress and extracellular polymeric substance formation in *Rubrivivax benzoatilyticus* JA2. *J Hazard Mater* 385:121571. <https://doi.org/10.1016/j.jhazmat.2019.121571>
- Peng H, Liang N, Li H, Chen F, Zhang D, Pan B, Xing B (2015) Contribution of coated humic acids calculated through their surface coverage on nano iron oxides for ofloxacin and norfloxacin sorption. *Environ Pollut* 204:191–198. <https://doi.org/10.1016/j.envpol.2015.04.029>
- Qian G, Xu L, Li N, Wang K, Qu Y, Xu Y (2022) Enhanced arsenic migration in tailings soil with the addition of humic acid, fulvic acid and thiol-modified humic acid. *Chemosphere* 286:131784. <https://doi.org/10.1016/j.chemosphere.2021.131784>
- Qu C, Chen W, Hu X, Cai P, Chen C, Yu X, Huang Q (2019) Heavy metal behaviour at mineral-organ interfaces: mechanisms, modelling and influence factors. *Environ Int* 131:104995. <https://doi.org/10.1016/j.envint.2019.104995>
- Ren J, Ren X, Chen J, Guo W, Yang B, Du P (2021) Humic-mineral interactions modulated by pH conditions in bauxite residues – implications in stable aggregate formation. *Geoderma* 385:114856. <https://doi.org/10.1016/j.geoderma.2020.114856>
- Ruan X, Zhu L, Chen B, Qian G, Frost RL (2015) Combined ¹H NMR and LSER study for the compound-specific interactions between organic contaminants and organobentonites. *J Colloid Interface Sci* 460:119–127. <https://doi.org/10.1016/j.jcis.2015.08.034>
- Sabah E, Ouki S (2017) Sepiolite and sepiolite-bound humic acid interactions in alkaline media and the mechanism of the formation of sepiolite-humic acid complexes. *Int J Miner Process* 162:69–80. <https://doi.org/10.1016/j.minpro.2017.03.005>
- Sander M, Pignatello J (2005) Characterization of charcoal adsorption sites for aromatic compounds: insights drawn from single-solute and bi-solute competitive experiments. *Environ Sci Technol* 39(6):1606–1615. <https://doi.org/10.1021/es0491351>
- Sissou Z, Liu H, Zhou H (2019) Transport velocities of aniline and nitrobenzene in sandy sediment. *J Soils Sediments* 19:2570–2579. <https://doi.org/10.1007/s11368-019-02287-6>
- Sun Q, Meng J, Sarkar B, Lan Y, Lin L, Li H, Yang X, Yang T, Chen W, Wang H (2020) Long-term influence of maize stover and its derived biochar on soil structure and organo-mineral complexes in Northeast China. *Environ Sci Pollut Res* 27(22):28374–28383. <https://doi.org/10.1007/s11356-020-08171-y>
- Sun W, Li Y, McGuinness LR, Luo S, Huang W, Kerkhof LJ, Mack E, Häggblom MM, Fennell DE (2015) Identification of anaerobic aniline-degrading bacteria at a contaminated industrial site. *Environ Sci Technol* 49(18):11079–11088. <https://doi.org/10.1021/acs.est.5b02166>
- Tang Z, Li Y, Yang Z, Liu D, Tang M, Yang S, Tang Y (2019) Characteristic and mechanism of sorption and desorption of benzene on humic acid. *Environ Sci Pollut Res* 26(20):20277–20285. <https://doi.org/10.1007/s11356-019-05095-0>
- Turlapati SA, Minocha R, Long S, Ramsdell J, Minocha SC (2015) Oligotyping reveals stronger relationship of organic soil bacterial community structure with N-amendments and soil chemistry in comparison to that of mineral soil at Harvard Forest, MA, USA. *Front Microbiol* 6. <https://doi.org/10.3389/fmicb.2015.00049>
- von Oepen B, Kördel W, Klein W (1991) Sorption of nonpolar and polar compounds to soils: processes, measurements and experience with the applicability of the modified OECD-Guideline 106. *Chemosphere* 22(3):285–304. [https://doi.org/10.1016/0045-6535\(91\)90318-8](https://doi.org/10.1016/0045-6535(91)90318-8)
- Wang F, He J, He B, Zhu X, Qiao X, Peng L (2018) Formation process and mechanism of humic acid-kaolin complex determined by carbamazepine sorption experiments and various characterization methods. *J Environ Sci* 69:251–260. <https://doi.org/10.1016/j.jes.2017.10.020>
- Wang L, Li X, Tsang DCW, Jin F, Hou D (2020) Green remediation of Cd and Hg contaminated soil using humic acid modified montmorillonite: immobilization performance under accelerated ageing conditions. *J Hazard Mater* 387:122005. <https://doi.org/10.1016/j.jhazmat.2019.122005>
- Wen X, Du C, Wan J, Zeng G, Huang D, Yin L, Deng R, Tan S, Zhang J (2019) Immobilizing laccase on kaolinite and its application in treatment of malachite green effluent with the coexistence of Cd (II). *Chemosphere* 217:843–850. <https://doi.org/10.1016/j.chemosphere.2018.11.073>
- Xu N, Huangfu X, Li Z, Wu Z, Li D, Zhang M (2019) Nanoaggregates of silica with kaolinite and montmorillonite: sedimentation and transport. *Sci Total Environ* 669:893–902. <https://doi.org/10.1016/j.scitotenv.2019.03.099>
- Xu P, Wu J, Wang H, Tang S, Cheng W, Li M, Bu R, Han S, Geng M (2022) Combined application of chemical fertilizer with green

- manure increased the stabilization of organic carbon in the organo-mineral complexes of paddy soil. *Environ Sci Pollut Res*. <https://doi.org/10.1007/s11356-022-22315-2>
- Yang K, Yan X, Xu J, Jiang L, Wu W (2021) Sorption of organic compounds by pyrolyzed humic acids. *Sci Total Environ* 781:146646. <https://doi.org/10.1016/j.scitotenv.2021.146646>
- Yeasmin S, Singh B, Kookana RS, Farrell M, Sparks DL, Johnston CT (2014) Influence of mineral characteristics on the retention of low molecular weight organic compounds: a batch sorption–desorption and ATR-FTIR study. *J Colloid Interface Sci* 432:246–257. <https://doi.org/10.1016/j.jcis.2014.06.036>
- Yousef RI, El-Eswed B, Al-Muhtaseb AAH (2011) Adsorption characteristics of natural zeolites as solid adsorbents for phenol removal from aqueous solutions: kinetics, mechanism, and thermodynamics studies. *Chem Eng J* 171(3):1143–1149. <https://doi.org/10.1016/j.cej.2011.05.012>
- Zhang S, Shao T, Bekaroglu SSK, Karanfil T (2010) Adsorption of synthetic organic chemicals by carbon nanotubes: effects of background solution chemistry. *Water Res* 44(6):2067–2074. <https://doi.org/10.1016/j.watres.2009.12.017>
- Zhou W, Yang Q, Chen C, Wu Q, Zhu L (2015) Fixed-bed study and modeling of selective phenanthrene removal from surfactant solutions. *Colloids Surf A* 470:100–107. <https://doi.org/10.1016/j.colsurfa.2015.01.077>
- Zhu X, He J, Su S, Zhang X, Wang F (2016) Concept model of the formation process of humic acid–kaolin complexes deduced by trichloroethylene sorption experiments and various characterizations. *Chemosphere* 151:116–123. <https://doi.org/10.1016/j.chemosphere.2016.02.068>

Publisher's note Springer Nature remains neutral with regard to jurisdictional claims in published maps and institutional affiliations.

Springer Nature or its licensor (e.g. a society or other partner) holds exclusive rights to this article under a publishing agreement with the author(s) or other rightsholder(s); author self-archiving of the accepted manuscript version of this article is solely governed by the terms of such publishing agreement and applicable law.